35th Annual International Conference of the IEEE EMBS
Osaka, Japan, 3 - 7 July, 2013

Experimental Implementation of a New Method of Imaging Anisotropic Electric Conductivities

Weijing Ma, *Member, IEEE,* Tim P. DeMonte, *Member, IEEE*, Adrian I. Nachman, Nahla M. H. Elsaid, Michael L. G. Joy, *Member, IEEE*

***Abstract*—This paper presents the first experiment of imaging anisotropic impedance using a novel technique called Diffusion Tensor Current Density Impedance Imaging (DT-CD-II). A biological anisotropic tissue phantom was constructed and an experimental implementation of the new method was performed. The results show that DT-CD-II is an effective way of non-invasively measuring anisotropic conductivity in biological media. The cross-property factor between the diffusion tensor and the conductivity tensor has been carefully determined from the experimental data, and shown to be spatially inhomogeneous. The results show that this novel imaging approach has the potential to provide valuable new information on tissue properties.**

I. Introduction

Diffusion Tensor Current Density Impedance Imaging (DT-CD-II) is a novel imaging technique that measures anisotropic conductivity. It utilizes both the diffusion tensor and current density information of the imaging subject [1].

Motivated by significant potential impact in cardiac imaging, breast cancer detection and other diagnostic applications, there has been considerable amount of research devoted to non-invasively imaging biological conductivity. The classical approach has been that of Electrical Impedance Tomography (EIT) [2]. This technique relies on multiple current and potential measurements on the body surface and the solution of a very ill-posed non-linear inverse problem. EIT is cost-efficient, fast and provides good contrast between different tissues. However, the ill-posedness of the underlying problem results in images of very low resolution, which decreases rapidly with the distance from the measurement boundary [3]. To overcome this severe limitation, it is natural to seek ways to obtain interior data, rather than relying only on boundary measurements. A number of hybrid methods have been proposed to achieve this goal, and to combine the good contrast of EIT with the high resolution of other imaging modalities. These include numerous works which use interior information that can be obtained using Magnetic Resonance Imaging (MRI) (see [4] for an extensive review) or various ultrasound-based approaches, such as Acousto-Electrical Tomography [5-7], Impedance-Acoustic Tomography [8] and Magnetoacoustic Imaging [9]. The new technique considered here builds on Current Density Impedance Imaging (CDII [10]), a conductivity imaging method we developed based on early work at the University of Toronto on measuring current density (CDI [11, 12]) using MRI phase information. (See also [13] for a review of recent advances in CDII.)

Most existing electric impedance imaging techniques assume that the conductivity is isotropic. While this assumption simplifies the problem it does not apply for many important electrically active tissues such as cardiac muscle, nerve tissue and skeletal muscle [14]. Imaging anisotropic conductivity of biological tissues is an important problem. An iterative procedure has been proposed in [15], and tested on some two dimensional simulations. As well, there has been recent progress when the data consists of power densities obtainable by ultrasound-modulated EIT [16]. However, to our knowledge, no hybrid experimental technique for non-invasive anisotropic conductivity measurement has been demonstrated.

Use of the diffusion tensor has been proposed to determine the conductivity tensor [17, 18]. The premise of these approaches is that both the electrical current conduction and water molecule diffusion are correlated through cross-property relations reflecting the underlying tissue structure. Sen *et al.* proposed that the two phenomena share the same statistical microstructure parameters [17], while Tuch *et al.* showed that the two tensors have the same eigenvectors [18]. The most recent development of such methods further proposed a linear relationship between the eigenvalues of the diffusion tensor and those of the conductivity tensor [18, 19].

The new DT-CD-II method is also based on the cross-property correlation between the diffusion tensor and the conductivity tensor. However, we treat the cross-property factor as unknown, and possibly spatially varying, to allow for tissue inhomogeneities. We then propose a quantitative method to determine it experimentally. The combination of the structural information from the diffusion tensor with inversion of the cross-property factor from electromagnetic measurements yields a new technique for imaging anisotropic conductivities.

*Research supported by NSERC Discovery Grants and a Mitacs Postdoctoral Fellowship.

W. Ma is with the Department of Electrical and Computer Engineering, University of Toronto, Toronto, ON M5S 3G9, Canada. (phone: 416-857-5386; e-mail: weijing.ma@utoronto.ca).

T. P. DeMonte was with University of Toronto, Toronto, ON M5S 3G9 Canada. He is now with FieldMetrica Inc. Canada (e-mail: tdemonte@fieldmetrica.com).

N. M. H. Elsaid is with Institute of Biomaterials and Biomedical Engineering, University of Toronto, Toronto, ON M5S 3G9, Canada (e-mail: nahola@gmail.com).

A. I. Nachman is with the Department of Mathematics and with the Department of Electrical and Computer Engineering, University of Toronto, Toronto, ON M5S 3G9, Canada (e-mail: nachman@math.toronto.edu)

M. L. G. Joy is with the Department of Electrical and Computer Engineering, University of Toronto, Toronto, ON M5S 3G9, Canada (e-mail: mike.joy@utoronto.ca)

978-1-4577-0216-7/13/$26.00 ©2013 IEEE

II. Theory

A. Measurement of the Diffusion Tensor

Diffusion Tensor Imaging (DTI) is an MR technique that can characterize the restricted diffusion properties of water molecules in tissue [20].

In DTI, the diffusion coefficient is modeled as a 3×3 tensor $\mathbf{D}$:

$$\mathbf{D}=\begin{pmatrix} D_{11} & D_{12} & D_{13} \\ D_{21} & D_{22} & D_{23} \\ D_{31} & D_{32} & D_{33} \end{pmatrix}. \quad (1)$$

The (spatially dependent) eigenvalues and eigenvectors of $\mathbf{D}$ represent the diffusion coefficient in the different directions at each location, and provide valuable information about the underlying tissue microstructure. This underlying tissue structure also determines its anisotropic conductivity properties.

B. Current Density Measurements

Current Density Imaging (CDI) is a MR based imaging modality which is able to non-invasively measure the current density inside a sample[11, 12]. CDI assumes that thelow frequency currents flow through a passive reciprocal material and that Ampere's law applies:

$$\nabla\times\mathbf{H}=\mathbf{J}. \quad (2)$$

Here, $\mathbf{J}$ is the current density field and $\mathbf{H}$ is the corresponding magnetic field.

An important advantage of CDI is that it requires no assumption about the isotropy of the material. Details of how the magnetic field and current density field measurements are obtained can be found in [11, 12].

C. Determination of the Cross-property Factor Relating the Conductivity Tensor to the Diffusion Tensor

Similar to (1), the anisotropic conductivity is modeled as a 3×3 positive definite matrix-valued function of position:

$$\boldsymbol{\sigma}=\begin{pmatrix} \sigma_{11} & \sigma_{12} & \sigma_{13} \\ \sigma_{21} & \sigma_{22} & \sigma_{23} \\ \sigma_{31} & \sigma_{32} & \sigma_{33} \end{pmatrix}. \quad (3)$$

We write the linear cross-property relation between $\boldsymbol{\sigma}$ and $\mathbf{D}$ as:

$$\boldsymbol{\sigma}(\mathbf{r})=c(\mathbf{r})\mathbf{D}(\mathbf{r}). \quad (4)$$

Here $c(\mathbf{r})$ is the cross-property factor. It is a scalar-valued quantity that describes the cross-property relation between the diffusion tensor and the conductivity tensor.

We seek to determine the unknown factor $c(\mathbf{r})$ from experimental measurement of the diffusion coefficient and of two currents $\mathbf{J}_1$ and $\mathbf{J}_2$. Mathematically, by multiplying by the inverse of the measured matrix $\mathbf{D}$, the problem can be reduced to one which is formally similar to that of determining an isotropic conductivity from two (modified) currents. A derivation similar to that in [10] then yields the following formula for the cross-property factor $c(\mathbf{r})$, valid at all points where the two currents are not parallel:

$$\nabla\ln c(\mathbf{r})=\frac{\nabla\times\mathbf{K}_2\cdot(\mathbf{K}_1\times\mathbf{K}_2)}{|\mathbf{K}_1\times\mathbf{K}_2|^2}\mathbf{K}_1+\frac{\nabla\times\mathbf{K}_1\cdot(\mathbf{K}_2\times\mathbf{K}_1)}{|\mathbf{K}_1\times\mathbf{K}_2|^2}\mathbf{K}_2+\frac{\nabla\times\mathbf{K}_1\cdot\mathbf{K}_2}{|\mathbf{K}_1\times\mathbf{K}_2|^2}\mathbf{K}_1\times\mathbf{K}_2. \quad (5)$$

Here $\mathbf{K}_1$ and $\mathbf{K}_2$ are diffusion modulated "pseudo"-currents:

$$\mathbf{K}_1(\mathbf{r})=(\mathbf{D}(\mathbf{r}))^{-1}\mathbf{J}_1,\quad \mathbf{K}_2(\mathbf{r})=(\mathbf{D}(\mathbf{r}))^{-1}\mathbf{J}_2. \quad (6)$$

III. Experimental Methods

A. Phantom Construction

An acrylic phantom was constructed in order to perform experiments to determine the accuracy, noise tolerance and spatial resolution of DT-CD-II. For current delivery, four circular platinum electrodes (15.0 mm in diameter, 0.4mm in thickness) were placed near the four corners of one face of the pineapple phantom (see Fig.1). Placing all four electrodes on one side of the object tests the resolution of the imaging method away from the measurement boundary. Platinum electrodes were used because of the smaller resulting susceptibility artifact as well as their resistance to electrical corrosion. In Fig.1, the electrodes are marked in different colors (blue and red), with each color representing an electrode combination that was used in the current delivery. During the CDI experiment, the electrodes were held in place using a custom-engineered acrylic holder and were compressed against the pineapple to ensure good contact.

Inside the cylindrical acrylic phantom, a pineapple was used in a series of pilot experiments. The pineapple was chosen as it has both good conductivity properties, and is known to be a good DTI anisotropic test object. The dimensions of the pineapple cylinder were 14cm for the height and 10cm for the diameter.

B. DT-CD-II Imaging Protocols

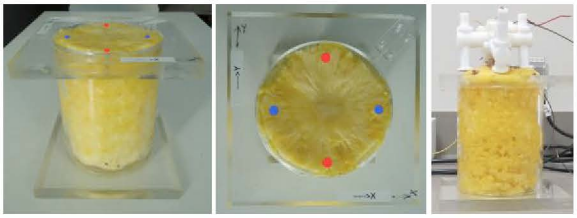

Figure1. Construction of the imaging phantom

The cylindrical acrylic phantom containing a large freshly cut pineapple specimen (140mm in height, 100mm in diameter). Four circular platinum plate electrodes (15.0mm in diameter, and 0.4mm in thickness) were positioned on one end of the pineapple for application of the currents. The electrodes were compressed against the pineapple to ensure good contact. The side and the bottom of the phantom remained watertight to prevent evaporation and leakage. Some air pockets remained.

Left: top configuration of the four electrodes; center: electrode positions; right: side view with attached electrode holder.

All experiments were conducted on a 1.5T GE® Signa MRI scanner. We used the stack DTI sequence based on the echo planar imaging (EPI) technique. A commercial eight

channel GE® birdcage head coil was used as the transmit/receive coil. To reduce the warping artifacts inherited from the EPI sequence, the ASSET parallel imaging technique was implemented. Sixteen repetitions were used to enhance the imaging quality. A B-value of 700 s/mm^2 was used to obtain an optimal balance between the effect of water diffusion in the pineapple fibers and the signal to noise ratio (SNR) of the image. The diffusion gradients were applied in six directions.

For CD acquisition, the same 1.5T GE® Signa MRI scanner was used. A standard birdcage coil was chosen to enhance the SNR of the acquired images. A fast gradient echo (FGRE) based low-frequency current density imaging (LFCDI) sequence was employed to measure two current density vector fields $\mathbf{J}_1$ and $\mathbf{J}_2$. Since CD acquisition requires rotations of the sample, the acrylic phantom was designed specifically to be stable under rotation. During the experiment, an 80mA current was applied to the phantom to create a change in the magnetic field and thus to probe the electrical property of the subject. Table 1 lists the MRI imaging parameters for both parts of the DT-CD-II experiment. The DTI images were mapped onto the same grid as the CDI imaging using the linear interpolation in the longitudinal direction and under-sampling in the transverse plane.

Table 1 MRI imaging parameters

Imaging type	Voxel size (mm^3)	TR (ms)	TE (ms)	Current (mA)	Slice number	Base sequence
DT	0.94x0.94x5.7	8000	86.4	N/A	26	EPI
CD	1.9x1.9x1.9	8.46	6.55	80	126	f-GRE

IV. Results

A. DTI Results and Pineapple Fiber Directions.

As the DTI experiment was conducted, dicom files were collected and used as input for a DTI processing software (DTIstudio). Fig. 2 shows the resulting eigenvectors and eigenvalues of the diffusion tensor in a slice of the 3D dataset (slice number =17).

Using the primary diffusion direction measured and shown (for one slice) in the top row of Fig. 2, the fibers are plotted using integration and fiber tracking techniques. Fig. 3 shows the 3D fiber trajectories inside the pineapple. On the left (Fig. 3.a) is the view from the top of the phantom, on the right (Fig. 3.b) is the cross sectional view. We observe that at the center of the pineapple, the fiber direction is mostly vertical. This corresponds to the fact that pineapple core has a distinctively different fibrous structure compared to the rest of the fruit. Away from the core, fibers in the peripheral flesh extend out essentially in the radial direction. These DTI results show that the pineapple contains distinctive structural variations that provide a good test of both parts of the DT-CD-II technique.

B. CDI Results and Current Pathways

Two currents, $\mathbf{J}_1$ and $\mathbf{J}_2$ were injected into the phantom. For CDI data processing, MRI raw files were collected and a MATLAB based data processing software package (available at www.currentdensityimaging.org) was used to extract current density information. Once $\mathbf{J}_1$ and $\mathbf{J}_2$ were measured, a data visualization tool MayaVi was used to check the corresponding current pathways.

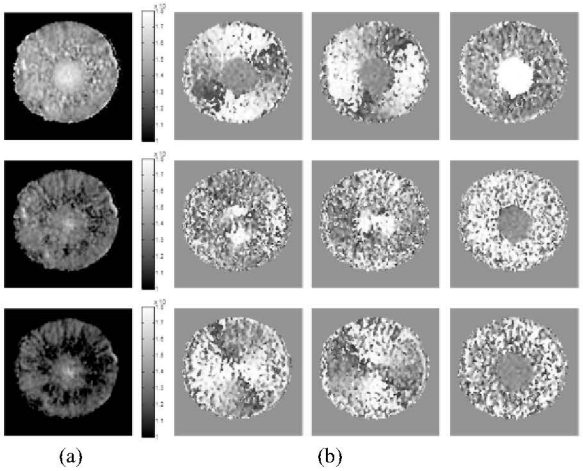

Figure 2. Eigenvalues and eigenvectors of the Diffusion Tensor for one slice

The figure shows the spatial dependence of the eigenvalues and eigenvectors of the diffusion tensor in slice 17 of the pineapple. From top to bottom: largest to smallest eigenvalues and their corresponding eigenvectors First Column shows the eigenvalues; second column: x component of the eigenvectors; third column: y component of the eigenvectors; fourth column: z component of the eigenvectors.

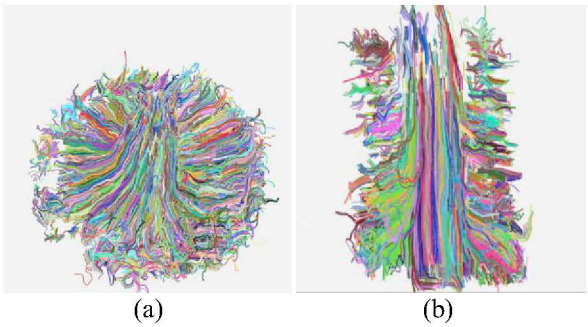

Figure3. Fiber trajectories generated using DTI

Fiber direction was constructed from the eigenvectors associated with the biggest eigenvalue. Each fiber is color-coded with a random color to differentiate from its neighboring fibers. (a) View from the top of the phantom; (b) cross-sectional view of the phantom. The fiber structure and variations are consistent with the biological facts of the pineapple anisotropy.

C. DT-CD-II Determination of the Anisotropic Conductivity Tensor

Using (5) (6) together with the current density and diffusion tensor measurements, $\nabla \ln c(\mathbf{r})$ was computed. Subsequently, the logarithm of the cross-property factor $c(\mathbf{r})$ was calculated through integration of its gradient field. Details of such computations can be found in [10].

Fig. 4 is the plot of $c(\mathbf{r})$ in slices from different depths of the pineapple phantom. It shows that at different depths and regions of the phantom, the cross-property factor is non-

uniform. This inhomogeneity of $c(\mathbf{r})$ proves that $\boldsymbol{\sigma}$ and $\mathbf{D}$ are not constant multiples of each other.

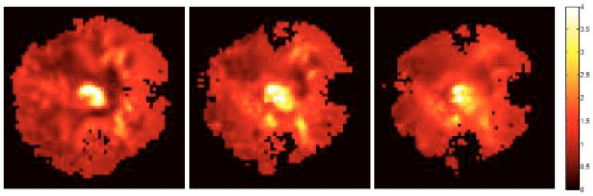

Figure 4. Measured cross-property factor $c(\mathbf{r})$ in different slices
Left: slice 16; middle: slice 18; right: slice 20. A bigger slice number indicates that the imaging plane is closer to the electrodes. The distance between the slices shown here is 10.4 *mm*.

Fig. 5 shows the computed conductivity $\boldsymbol{\sigma}$ using (4). The normalized standard deviation of diagonal entries of $\boldsymbol{\sigma}$ can be as high as 0.6 compared to those of $\mathbf{D}$ at 0.15. The differences in the variability of the off-diagonal entries of the diffusion tensor $\mathbf{D}$ is less pronounced compared to $\boldsymbol{\sigma}$.

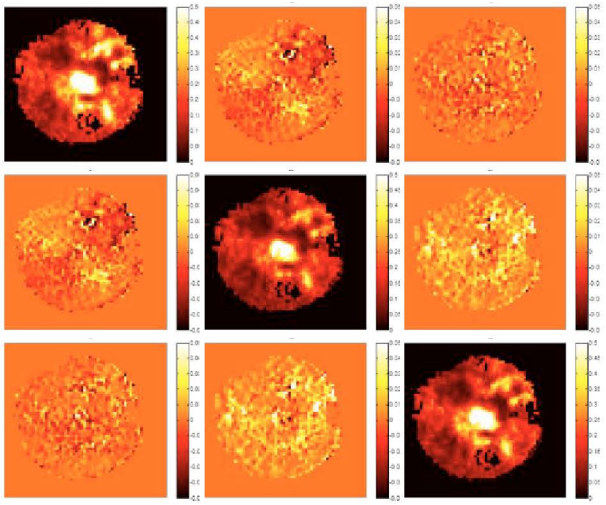

Figure 5. Conductivity tensor $\boldsymbol{\sigma}$ in slice 17
Each plot is a component of $\boldsymbol{\sigma}(i, j)$, where i is the row number and j is the column number. To illustrate the subtle variance in the off-diagonal components, the off diagonal components of $\boldsymbol{\sigma}(i, j)$ are drawn with dynamic range [-0.05,0.05], while the three diagonal components are drawn with dynamic range [0,0.5].

V. Discussion and Conclusion

In this work, a novel non-invasive technique (DT-CD-II) for imaging inhomogeneous anisotropic conductivities has been implemented experimentally for the first time. The results prove that even though $\boldsymbol{\sigma}$ and $\mathbf{D}$ are correlated through the underlying microstructure, the diffusion tensor $\mathbf{D}$ does not by itself image the conductivity tensor $\boldsymbol{\sigma}$. The cross-property factor which relates the two tensors turns out to have significant spatial inhomogeneity. The DT-CD-II method provides the first experimental procedure to determine precisely the spatial distribution of $c(\mathbf{r})$, and the corresponding anisotropic conductivity.

Acknowledgment

The authors thank Dr. M. Pop (Sunnybrook Hospital, Toronto, Canada), Dr. S. Chavez (Center for Addiction and Mental Health, Toronto, Canada) and Prof. M. Sussman (University Heath Network, Toronto, Canada) for very helpful discussions on DTI implementation.

References

[1]W. Ma, A. I. Nachman, N. Elsaid, M. L. G. Joy, and T. P. DeMonte, "Anisotropic Impedance Imaging Using Diffusion Tensor and Current Density Measurements," to be submitted.

[2]M. Cheney, D. Isaacson, and J. C. Newell, "Electrical impedance tomography," *Siam Review,* vol. 41, pp. 85-101, Mar 1999.

[3]D. Isaacson, "Distinguishability of Conductivities by Electrical-current Computed Tomography," *Ieee Transactions on Medical Imaging,* vol. 5, pp. 91-95, Jun 1986.

[4]J. K. Seo, D. H. Kim, J. Lee, O. I. Kwon, S. Z. K. Sajib, and E. J. Woo, "Electrical tissue property imaging using MRI at dc and Larmor frequency," *Inverse Problems,* vol. 28, Aug 2012.

[5]H. Zhang and L. V. Wang, "Acousto-electric tomography," in *Photons Plus Ultrasound: Imaging and Sensing*. vol. 5320, A. A. Oraevsky and L. V. Wang, Eds., ed Bellingham: Spie-Int Soc Optical Engineering, 2004, pp. 145-149.

[6]H. Ammari, E. Bonnetier, Y. Capdeboscq, M. Tanter, and M. Fink, "Electrical impedance tomography by elastic deformation," *Siam Journal on Applied Mathematics,* vol. 68, pp. 1557-1573, 2008.

[7]P. Kuchment and L. Kunyansky, "Synthetic Focusing in Ultrasound Modulated Tomography," *Inverse Problems and Imaging,* vol. 4, pp. 665-673, Nov 2010.

[8]B. Gebauer and O. Scherzer, "Impedance-acoustic Tomography," *Siam Journal on Applied Mathematics,* vol. 69, pp. 565-576, 2008.

[9]G. Hu and B. He, "Magnetoacoustic Imaging of Electrical Conductivity of Biological Tissues at a Spatial Resolution Better than 2 mm," *Plos One,* vol. 6, Aug 2011.

[10]K. F. Hasanov, A. W. Ma, A. I. Nachman, and M. L. Joy, "Current density impedance imaging," *IEEE Trans Med Imaging,* vol. 27, pp. 1301-9, Sep 2008.

[11]M. L. G. Joy, G. C. Scott, and R. M. Henkelman, "In-Vivo Detection of Applied Electric Currents by Magnetic Resonance Imaging," *Magnetic Resonance Imaging,* vol. 7, pp. 89-94, 1989.

[12]G. C. Scott, M. L. G. Joy, R. L. Armstrong, and R. M. Henkelman, "Measurement of nonuniform current density by magnetic resonance," *IEEE Trans. Med. Imag,* vol. 10, pp. 362-374, 1991.

[13]A. Nachman, A. Tamasan, and A. Timonov, "Current Density Impedance Imaging," in *Tomography and Inverse Transport Theory*. vol. 559, G. Bal, D. Finch, P. Kuchment, J. Schotland, P. Stefanov, and G. Uhlmann, Eds., ed Providence: Amer Mathematical Soc, 2011, pp. 135-149.

[14]D. Gullmar, J. Haueisen, and J. R. Reichenbach, "Influence of anisotropic electrical conductivity in white matter tissue on the EEG/MEG forward and inverse solution. A high-resolution whole head simulation study," *Neuroimage,* vol. 51, pp. 145-63, May 15 2010.

[15]J. K. Seo, F. C. Pyo, C. Park, O. Kwon, and E. J. Woo, "Image reconstruction of anisotropic conductivity tensor distribution in MREIT: computer simulation study," *Physics in Medicine and Biology,* vol. 49, pp. 4371-4382, Sep 2004.

[16]F. Monard and G. Bal, "Inverse anisotropic conductivity from power densities in dimension n ≥ 3," preprint, submitted in Aug. 2012.

[17]A. K. Sen and S. Torquato, "Effective Conductivity of Anisotropic 2-phase Composite Media," *Physical Review B,* vol. 39, pp. 4504-4515, Mar 1989.

[18]D. S. Tuch, V. J. Wedeen, A. M. Dale, J. S. George, and J. W. Belliveau, "Conductivity tensor mapping of the human brain using diffusion tensor MRI," *Proceedings of the National Academy of Sciences of the United States of America,* vol. 98, pp. 11697-11701, Sep 2001.

[19]D. S. Tuch, V. J. Wedeen, A. M. Dale, J. S. George, and J. W. Belliveau, "Conductivity Mapping of Biological Tissue Using Diffusion MRI," *Annals of the New York Academy of Sciences,* vol. 888, pp. 314-316, 1999.

[20]D. Lebihan, E. Breton, D. Lallemand, P. Grenier, E. Cabanis, and M. Lavaljeantet, "MR Imaging of Intravoxel Incoherent Motions - Application to Diffusion and Perfusion in Neurologic Disorders," *Radiology,* vol. 161, pp. 401-407, Nov 1986.